What Is the Hidden Depolarization Mechanism in Low-luminosity AGNs?

Bower, G.C.; Dexter, J.; Markoff, S.; Rao, R; Plambeck, R.L.

DOI
10.3847/2041-8213/aa7b2e
Publication date
2017
Document Version
Author accepted manuscript
Published in
Astrophysical Journal Letters

What is the Hidden Depolarization Mechanism in Low Luminosity AGN?

Geoffrey C. Bower,[1] Jason Dexter,[2] Sera Markoff,[3] Ramprasad Rao,[1] R. L. Plambeck[4]

ABSTRACT

Millimeter wavelength polarimetry of accreting black hole systems can provide a tomographic probe of the accretion flow on a wide range of linear scales. We searched for linear polarization in two low luminosity active galactic nuclei (LLAGN), M81 and M84, using the Combined Array for Millimeter Astronomy (CARMA) and the Submillimeter Array (SMA). We find upper limits of $\sim 1-2\%$ averaging over the full bandwidth and with a rotation measure (RM) synthesis technique. These low polarization fractions, along with similar low values for LLAGN M87 and 3C84, suggest that LLAGN have qualitatively different polarization properties than radio-loud sources and Sgr A*. If the sources are intrinsically polarized and then depolarized by Faraday rotation then we place lower limits on the RM of a few times 10^7 rad m^{-2} for the full bandwidth case and $\sim 10^9$ rad m^{-2} for the RM synthesis analysis. These limits are inconsistent with or marginally consistent with expected accretion flow properties. Alternatively, the sources may be depolarized by cold electrons within a few Schwarzschild radii from the black hole, as suggested by numerical models.

Subject headings: black hole physics, accretion, galaxies: jets, galaxies: active

1. Introduction

Models of black hole accretion span many orders of magnitude in linear scale but observational constraints tend to probe only very narrow ranges, predominantly in regions where

[1]Academia Sinica Institute of Astronomy and Astrophysics, 645 N. A'ohoku Place, Hilo, HI 96720, USA; gbower@asiaa.sinica.edu.tw

[2]Max Planck Institute for Extraterrestrial Physics, Giessenbachstr. 1, 85748 Garching, Germany

[3]Anton Pannekoek Institute for Astronomy, University of Amsterdam, Science Park 904, 1098 XH Amsterdam, The Netherlands

[4]Radio Astronomy Laboratory, University of California, Berkeley, CA 94720-3411, USA

emission arises (Yuan & Narayan 2014). Faraday rotation provides a unique line-of-sight probe that can measure the integral properties of accretion flows over a wide range of radii and physical conditions. A magnetized plasma rotates the plane of linear polarization by an angle that is proportional to the rotation measure (RM), which is the line-of-sight integral of the electron density and the parallel component of the magnetic field. In cases where linearly polarized emission arises near the black hole, Faraday rotation can probe scales ranging from a few to thousands (or more) of Schwarzschild radii (R_S).

Millimeter wavelength observations are well-suited to probing accretion flows around supermassive black holes. At these wavelengths, emission regions tend to be compact and originate from near the black hole. Further, the short wavelengths provide sensitivity to large RMs $\gtrsim 10^6$ rad m^{-2}, which are characteristic of accretion flow models for many systems. At longer wavelengths, intrinsically polarized sources will be quickly depolarized through bandwidth or beam depolarization mechanisms (e.g., Bower et al. 1999).

Millimeter wavelength polarimetric probes of the accretion flow were first developed for Sgr A* (Bower et al. 2003; Marrone et al. 2007) and have since been applied to M87 (Kuo et al. 2014) and 3C 84 (Plambeck et al. 2014). In the case of Sgr A*, the detected RM $\sim -5 \times 10^5$ rad m^{-2} sets a constraint on the accretion rate of $\dot{M} \sim 10^{-8\pm1}$ M$_\odot$ y^{-1} and rules out canonical, loss-free advection dominated accretion flows (ADAFs; Narayan & Yi 1995). Time variability of the RM can be used as a tomographic probe of structures in the accretion flow (Bower et al. 2005; Pang et al. 2011).

In this paper, we apply the technique of millimeter wavelength polarimetry to two nearby low luminosity AGN (LLAGN), M81 and M84. Both of these sources have been studied extensively across the electromagnetic spectrum (e.g., Bietenholz et al. 2000; Ly et al. 2004; Markoff et al. 2008; Bower et al. 2015; Russell et al. 2013). Dynamical black hole masses have been determined for both M81 and M84 to be $6.5 \times 10^7 M_\odot$ and $8.3 \times 10^8 M_\odot$, respectively (Kormendy & Ho 2013). In Section 2, we present observations obtained with the Combined Array for Research in Millimeter-wave Astronomy (CARMA) and the Submillimeter Array (SMA). In Section 3, we present our results and analysis. In Sections 4 and 5, we discuss these results and provide our conclusions.

2. Observations

2.1. CARMA Observations of M81

M81 data were obtained with the CARMA D-array on 2013 Feb 18 in good weather (3mm precipitable water). Observations of M81 were interleaved with those of the phase

calibrator, 0958+655; 3C 84 was used as a passband calibrator. The synthesized beam size on M81 was 2.6×2.4 arcsec in position angle 58 deg East of North. The 8 hour observing track covered a parallactic angle range of 160 degrees (-100 to -180/+180 to +100) for M81. The dual-polarization receivers are equipped with broadband waveguide circular polarizers and orthomode transducers, allowing simultaneous observations of right (R) and left (L) circular polarization (Hull & Plambeck 2015). The CARMA correlator was configured to process two 2 GHz wide frequency bands, centered at 216.6 GHz in the receivers' lower sideband and 231.1 GHz in the upper sideband. The correlator provided 0.0104 GHz frequency resolution for all four cross-polarizations (RR,LL,RL,LR)

Polarization leakage corrections were derived from a 5-hour observation of 3C 279 one month later, on 2013 Mar 18, that covered a 75 degree range in parallactic angle. The observing frequency and correlator configuration were identical to those used for M81. There are no moving parts in the dual polarization receivers, and the leakage corrections are known to be stable over periods of many months. The leakage corrections compensate for cross-coupling between the R and L channels. As discussed by Hull & Plambeck (2015), reflections within the receivers cause ripples on scales of $\sim$ 100 MHz on some of the telescopes. For normal broadband observations of dust polarization (e.g., Hull et al. 2014) these ripples average out, but for RM synthesis we take care to derive and apply the leakage corrections independently for each 0.052 GHz wide frequency interval before calculating Stokes I,Q,U,V for that interval.

2.2. SMA Observations of M84

The SMA data on M84 were taken on three different epochs, 30 Jan 2016, 21 Feb 2016, and 29 Feb 2016. The weather conditions were excellent on all three days with the 225 GHz atmospheric opacity between 0.02 and 0.04 (precipitable water vapor below 0.5 mm to 1 mm). The primary phase calibrator was 3C 273 which was also used to calibrate the passband and instrumental polarization. The observing time on M84 on each of the days was $\sim$7 hours while the parallactic angle coverage was $\sim$160 degrees (-90 degrees to +70 degrees). The SMA observed in a double sideband mode with the upper sideband covering a frequency range from 230.9 GHz to 234.9 GHz while the lower sideband covered a frequency range from 218.9 GHz to 222.9 GHz. The correlator was set to a frequency resolution of $\sim$3 MHz. The instrumental polarizations or leakages were derived from 3C 273 which was observed simultaneously with the target observations of M84 (Marrone & Rao 2008). The parallactic angle coverage was similar to that of the target M84 (i.e., 160 degrees).

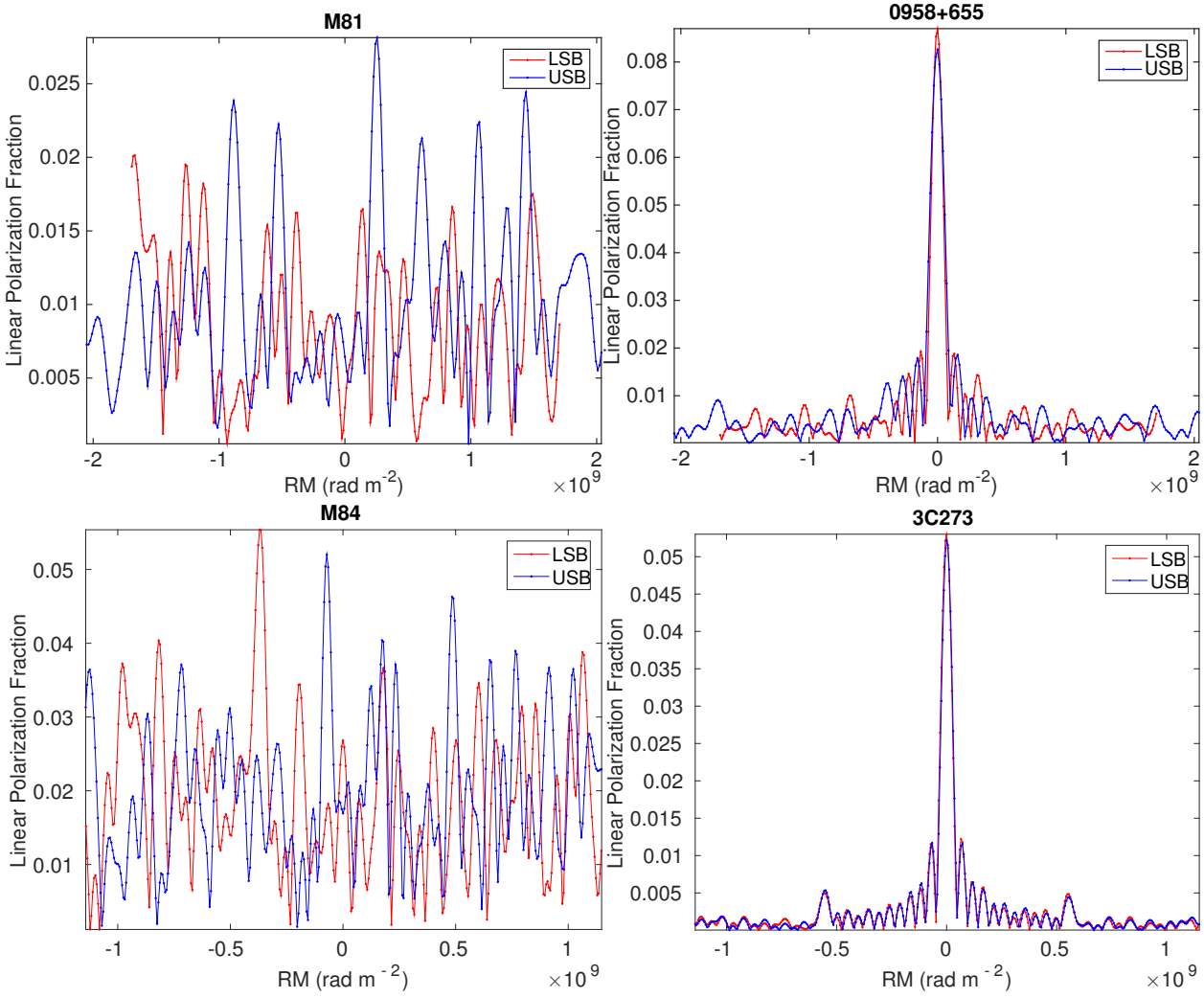

Fig. 1.— Rotation measure synthesis results for M81 (upper left), M84 (lower left), 0958+655 (upper right), and 3C 273 (lower right). Results show the linear polarization fraction as a function of RM for the upper and lower sidebands. The M84 results are from the most sensitive epoch, 160221. The results for the calibrators 0958+655 and 3C 273 are consistent with RM = 0 rad m^{-2}. No detection is made for either M81 or M84 in any epoch.

3. Results and Analysis

We summarize our polarimetric results for M81, M84, and their calibrators in Table 1. Results are tabulated per epoch for each sideband in Stokes I, Q, and U parameters. No polarized emission is detected from either M81 or M84. There are no detections for either source in upper or lower sidebands or in the average of the two sidebands. Further, M84 is not detected in any epoch, as well as not in the average over all epochs and sidebands. The calibrators 0958+655 and 3C273 are clearly detected in all sidebands and epochs with consistent values.

We also searched spectral data for RMs up to a maximum

$$\mathrm{RM}_{lim} = \frac{\pi}{2\lambda^2}\frac{\nu}{\Delta\nu}, \tag{1}$$

where λ and ν refer to observing wavelength and frequency, and $\Delta\nu$ is the channel width (Brentjens & de Bruyn 2005). The M81 CARMA data were spectrally averaged into 36 channels of width 0.052 GHz in each sideband. The M84 SMA data were averaged in each of 48 spectral window of width 0.112 GHz. In the lower sideband, this spectral structure corresponds to $\mathrm{RM}_{lim} = 3.4 \times 10^9$ rad m^{-2} and 1.7×10^9 rad m^{-2} for M81 and M84, respectively. RM synthesis for the two calibrators revealed upper and lower sideband results both consistent with RM = 0 rad m^{-2}. The width of the RM transfer function is 4.7×10^7 rad m^{-2} and 2.3×10^7 rad m^{-2} for M81 and M84, respectively. No significant peaks were found in the RM spectra for M81 and M84 in any epoch (Figure 1). Upper limits are $\sim 2\%$ of the total intensity.

Under the assumption that M81 and M84 are intrinsically linearly polarized but appear unpolarized due to bandwidth depolarization, we place two lower limits on the RM. The first is based on the non-detection in either the lower or upper sideband averaged channels. For the case of 1 radian of rotation, the RM limits are 3.1×10^7 rad m^{-2} and 1.6×10^7 rad m^{-2} for M81 and M84, respectively. The second is based on non-detection in the RM spectra with the limits given above, $\sim 10^9$ rad m^{-2}. The fractional polarization limits from these two methods are comparable.

Whether the RM limit is physically applicable depends on the uniformity of the Faraday medium over the solid angle of the source. In this case, the large RM $\sim 10^9$ rad m^{-2} implies ~ 600 complete turns of phase at our observational wavelength. Inhomogeneities of a part in 10^3 in the Faraday medium could lead to beam depolarization. Models for Faraday rotation in the accretion flow discussed below are insufficiently detailed to provide any meaningful constraint on beam depolarization for the very compact size of the polarized emission.

4. Discussion

Millimeter wavelength radio-loud AGN have been shown to be strongly polarized (Trippe et al. 2010; Agudo et al. 2014). At 3.4 mm, surveys have shown a median fractional polarization of $\approx 4\%$ with values ranging as high as 19%. Polarized flux is detected in $\sim 90\%$ of sources at fractions above 1%. The average 3 mm polarization fraction is a factor ~ 2 times higher than the average polarization fraction at 2 cm. Surveys at 1.3 mm detect fewer polarized sources as a result of reduced sensitivity, but for those sources that are detected the mean polarization fraction increases by ~ 1.6 times relative to 3.4 mm. The results are consistent with a general trend of increased magnetic field order from the smaller source regions that are expected with decreasing wavelength.

The non-detection of polarization from the LLAGN M81 and M84, as well as the weak linear polarization detected from M87 and 3C 84, suggest that these sources are qualitatively different from the blazars and radio loud objects that make up the survey samples. These differences may arise from the very different radii at which the emission arises due to the beamed jet structure or from the effect of jet orientation. Further, the LLAGN polarization fractions appear to be qualitatively different from that of Sgr A*, which shows $\sim 10\%$ polarization fraction at mm wavelengths (Figure 2). This is in contrast with the consistent cm wavelength picture of the mm polarization of Sgr A* and M81: both exhibit undetected linear polarization along with detectable circular polarization (Brunthaler et al. 2001). We consider below whether the mm polarization differences can be accounted for with internal emission or extrinsic Farday effects, or some combination thereof.

The large RM towards Sgr A* has been successfully modeled as the result of propagation through the ionized, magnetized accretion flow (Bower et al. 2003; Marrone et al. 2007). The RM is directly tied to the mass accretion rate in these models. Generically, models make predictions for the accretion rate using radial profiles in electron density, $n_e \propto r^{\beta}$, and magnetic field strength, which is typically assumed to be in equipartition with the particle kinetic energy. ADAF models without winds or convection have centrally peaked profiles ($\beta = 3/2$) that have diminishing importance as the source of the emission moves further out; RIAF models ($\beta \approx 1/2$; Blandford & Begelman 1999) have a broad maximum in RM at larger radii and so are less sensitive to the location of the emission region. Exact RM predictions are a function of black hole mass (M_{bh}), mass accretion rate at the inner radius of the accretion flow ($\dot{M}$ in $M_{\odot}$ per year), and the inner and outer radii of the accretion flow

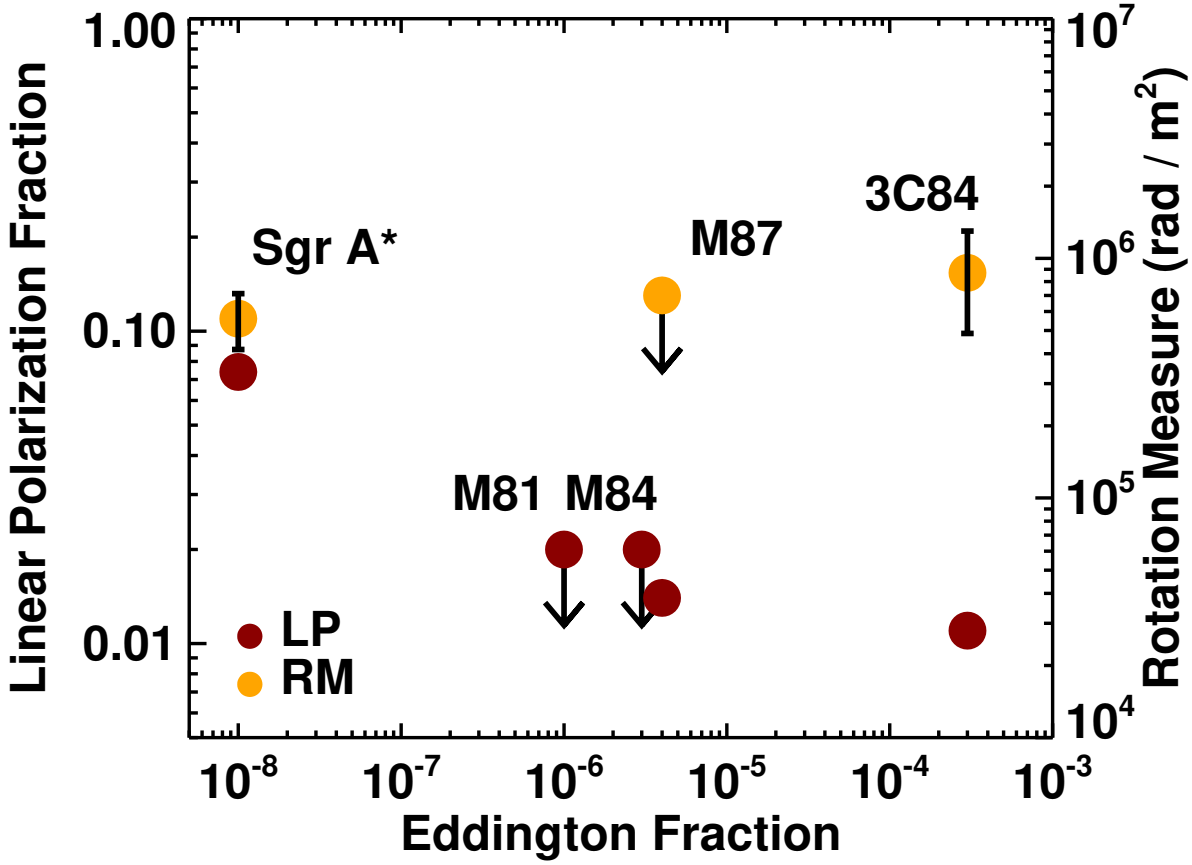

Fig. 2.— Linear polarization fraction (LP, red circles) and rotation measure (RM, yellow circles) as a function of the Eddington fraction, i.e., the ratio of bolometric luminosity to Eddington luminosity. The 3 available RM constraints show roughly constant values despite large differences in black hole mass and accretion rate. The measured LPs except for Sgr A* are also low compared to radio loud AGN. For M81 and M84, the low LP could be the result of beam or Faraday depolarization.

(r_{in}, r_{out} expressed in R_s; Marrone et al. 2006)[1]:

$$\mathrm{RM} \propto \left(\frac{2}{3\beta-1}\right)\left(1-\left(\frac{r_{out}}{r_{in}}\right)^{-(3\beta-1)/2}\right) r_{in}^{-7/4} M_{bh}^{-2}\dot{M}^{3/2}. \quad (2)$$

These models work well for Sgr A* and provide reasonable estimates for the case of M87 (Kuo et al. 2014) but underpredict the RM observed towards 3C 84 by orders of magnitude (Plambeck et al. 2014).

If we assume that M81 and M84 are intrinsically polarized but depolarized through the accretion medium, then we can place constraints on the accretion flow properties. Both M81 and M84 are compact sources with jet structure marginally resolved at sub-parsec resolution (Bietenholz et al. 2000; Ly et al. 2004; Markoff et al. 2008). In the case of M84, 7mm VLBA observations show that the source is compact on a scale of few hundred R_S. In the case of M81, a core with a compact jet is seen at a wavelength of 3.4 cm; the core has a maximum scale of $10^3 R_S$. If these sources resemble M87, then we expect the polarization to arise from even more compact regions, comparable to $\sim 10R_S$. Thus, it is reasonable to test the hypothesis that polarized emission is generated on small scales and then propagates through a geometrically thick (quasi-spherical) accretion flow, where it is depolarized.

In Figures 3 we plot our two RM limits against mass accretion rate, as well as expectations for ADAF and RIAF models with a range of inner and outer radii. We obtain the mass accretion rate for M81 from detailed spectral modeling, which treats the observed X-ray luminosity as primarily a non-thermal component associated with the jet (Markoff et al. 2008). The various M81 models are consistent with an accretion disk bolometric luminosity that is $10^{-6}L_{Edd}$, or an accretion rate of $10^{-6}\eta_{0.1}^{-1}M_\odot$ y^{-1}, where $\eta_{0.1}$ is the efficiency normalized by the thin-disk value of 0.1. We determine the instantaneous mass accretion rate for M84 based on the unabsorbed X-ray luminosity of the nucleus at 7×10^{-7} $M_\odot$ y^{-1} (Russell et al. 2013). A long-term average accretion rate of $2\times10^{-4}M_\odot$ y^{-1} for M84 has been also determined through analysis of the power required to create the observed X-ray cavity, which has a time scale $\sim 10^6$ y (Rafferty et al. 2006). Both M81 and M84 are known to show variable nuclear X-ray emission with up to an order of magnitude change in luminosity on time scales of months to years. Thus, the accretion rate for both sources may be uncertain by more than an order of magnitude.

In the case of M81, we see depolarization in the accretion flow is marginally consistent with RIAF and ADAF models. Those models must have cold (non-relativistic) electrons down to small radii, $r_{in} \approx 3$, to produce sufficient depolarization. Alternatively, clumpiness

[1]Note the corrected sign on the exponent for r_{in}.

at large radii or a higher long-term accretion rate could lead these results to be consistent with accretion theory. In the case of M84, for the current epoch accretion rate, both RIAF and ADAF models are strongly rejected. For the long-term average accretion rate, however, RIAF and ADAF models can be constructed that are consistent with non-detection of linear polarization.

It is unclear whether this simple picture of the intrinsically polarized source and external Faraday medium will hold in these sources. First, Sgr A* reveals significant complexity in its polarization on R_S scales, possibly as the result of spatially-variable magnetic-field structure (Johnson et al. 2015). Second, long wavelength RM synthesis observations of Sgr A* that were sensitive to $RM \leq 1.5 \times 10^7$ rad m^{-2} did not detect the polarization in spite of the fact that millimeter wavelength polarimetry detected a strongly polarized source at $RM = -5 \times 10^5$ rad m^{-2} (Bower et al. 1999). The absence of that detection is likely either due to beam depolarization for the much larger intrinsic source at long wavelengths, or to other effects that suppress the intrinsic polarization. In the case of Sgr A*, the polarized millimeter wavelength source may represent only the inner accretion flow or jet structure, whereas the long wavelength emission may represent a larger-scale jet or nonthermal particles in the larger-scale accretion flow. On the other hand, for both M81 and M84, like M87, the spectrum is consistent with a single source component that is associated with a self-similar jet.

We also consider the possibility that the sources are not intrinsically polarized. Given the compact source size of the emitting regions at these wavelengths, estimated to be tens of R_S, this requires a substantial degree of cancellation over a small area. Magnetic-field structure in Sgr A* appears to lead to a reduction from the peak polarized fraction to the average polarized fraction by a factor of several. Such a reduction still leaves a substantially polarized source. Both M81 and M84 show a steep spectrum indicative of optically thin emission, eliminating optically thick emission as a source for internal depolarization in the mm. A more plausible hypothesis is mixed thermal and nonthermal material within the emission region that leads to internal depolarization.

Numerical models using semi-analytic prescriptions for electron heating (Mościbrodzka et al. 2014, 2016; Ressler et al. 2017) can now self-consistently calculate polarized emission from low-luminosity accretion flows including internal and external Faraday effects at least out to $r \sim 100R_S$ (Dexter 2016; Mościbrodzka et al. 2017). The models can reproduce flat radio spectra from a self-absorbed jet (e.g., Blandford & Konigl 1979; Falcke & Biermann 1995). At 230 GHz the emission is predicted to originate from close to the event horizon, where the counter-jet is lensed into a crescent shape (Dexter et al. 2012). The LP from this configuration is typically only $\simeq 1-3\%$ as a result of either beam or Faraday depolarization

(Mościbrodzka et al. 2017), consistent with observations of M87 (Kuo et al. 2014).

In these numerical models, mildly relativistic or cold electrons near the black hole produce strong Faraday depolarization ($r_{\rm in} \sim R_S$) and large RM values when viewed at moderate to high inclinations, roughly in agreement with Equation 2. When viewed at low inclination (e.g. M87), the RM can be much lower than predicted, such that $\gtrsim 10\times$ higher accretion rates are consistent with the observations. At larger inclination, the RM is predicted to increase rapidly. The non-detections of LP in M81 and M84 are consistent with the Mościbrodzka et al. (2017) model predictions if the 230 GHz emission originates near the event horizon (as suggested for M81 by its short variability timescale, Bower et al. 2015). Future higher sensitivity observations could determine whether the RM is large (moderate to high inclination), or similar to that measured for M87, possibly indicating horizon scale counter-jet emission viewed at small inclination.

5. Conclusions

We have presented CARMA and SMA millimeter wavelength polarimetry measurements for the LLAGN M81 and M84. We detect no linear polarization from these sources in spite of the sensitivity to very large RMs. Interpreted through the model of a compact, intrinsically depolarized source that is depolarized by a homogeneous accretion flow that extends from close to the black hole to the Bondi radius, we find that the results are inconsistent or marginally consistent with other constraints on the accretion flow. Additional cold, depolarizing material near the black hole may be responsible for the depolarization.

These results, along with those for Sgr A*, M87, and 3C 84, demonstrate that LLAGN have different properties than we see for higher luminosity radio sources at these wavelengths. Study of a broader sample of objects over a wide range of wavelengths and at greater sensitivity with ALMA will be critical for understanding this tool for probing accretion flows and jets on scales of a few to thousands of Schwarzschild radii. Finally, in the case of the brightest sources, polarized imaging with the Event Horizon Telescope may produce maps of polarization structure that cannot be obtained in any other way.

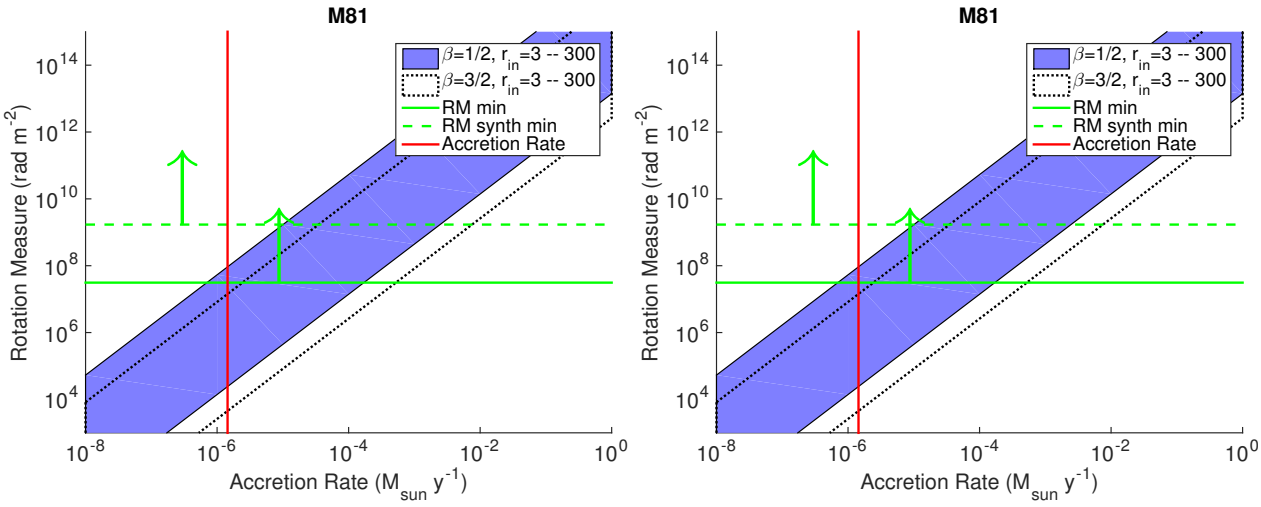

Fig. 3.— Rotation measure versus accretion rate for M81 (left) and M84 (right). The vertical red line is the inferred accretion rate from the X-ray luminosity. The horizontal green lines are the minimum RM to depolarize the source within each sideband (solid line) and within each channel (dashed line). The blue shaded region represents parameter space associated with RIAF models ($\beta = 1/2$) for $r_{in} = 3$ to 300. The space enclosed within the dotted lines represent parameter space associated with ADAF models ($\beta = 3/2$). Space to the upper left of the model curves is excluded. Additionally, we show a vertical red line indicating the long-term average for the M84 accretion rate.

Table 1. Polarimetric Results

Tel.	Epoch (yymmdd)	Source	ν (GHz)	I (mJy)	Q (mJy)	U (mJy)	P (mJy)
CARMA	130218	M81	216.6	75.0 ± 0.6	-0.2 ± 0.5	0.1 ± 0.6	0.2 ± 0.5
...	...	...	231.1	77.3 ± 0.8	-0.5 ± 0.6	0.0 ± 0.7	0.5 ± 0.6
...	...	...	Mean	76.1 ± 0.5	-0.3 ± 0.4	0.1 ± 0.5	0.4 ± 0.4
CARMA	130218	0958+655	216.6	698.8 ± 1.0	60.8 ± 1.1	-0.6 ± 1.3	60.8 ± 1.1
...	...	...	231.1	704.7 ± 1.3	58.2 ± 1.2	0.7 ± 1.7	58.2 ± 1.2
...	...	...	Mean	701.8 ± 0.8	59.5 ± 0.8	0.1 ± 1.0	59.5 ± 0.8
SMA	160130	M84	220.9	119.1 ± 1.6	-1.7 ± 1.3	-0.1 ± 1.6	1.7 ± 1.3
...	...	...	232.9	114.0 ± 1.4	-2.3 ± 1.4	0.5 ± 1.3	2.3 ± 1.4
...	...	...	Mean	116.5 ± 1.1	-2.0 ± 1.0	0.2 ± 1.0	2.0 ± 0.9
SMA	160130	3C273	220.9	9600.2 ± 4.3	67.1 ± 2.6	-382.0 ± 3.6	387.8 ± 3.5
...	...	...	232.9	9872.9 ± 3.1	102.1 ± 2.8	-317.3 ± 5.7	333.3 ± 5.5
...	...	...	Mean	9736.5 ± 2.5	84.6 ± 1.9	-349.7 ± 3.0	359.7 ± 3.0
SMA	160221	M84	220.9	129.4 ± 1.9	2.1 ± 1.9	-2.7 ± 2.1	3.5 ± 2.0
...	...	...	232.9	144.9 ± 1.8	-2.4 ± 2.5	-0.3 ± 2.1	2.5 ± 2.5
...	...	...	Mean	137.2 ± 1.3	-0.1 ± 1.5	-1.5 ± 1.5	1.5 ± 1.5
SMA	160221	3C273	220.9	12298.1 ± 49.3	339.5 ± 4.2	-556.5 ± 6.3	651.9 ± 5.8
...	...	...	232.9	11179.6 ± 19.9	317.2 ± 4.3	-489.4 ± 5.7	583.2 ± 5.4
...	...	...	Mean	11738.8 ± 18.5	328.4 ± 3.0	-523.0 ± 4.2	617.5 ± 3.9
SMA	160229	M84	220.9	160.0 ± 1.5	-0.9 ± 1.3	-2.0 ± 1.7	2.2 ± 1.7
...	...	...	232.9	171.3 ± 1.6	-2.7 ± 1.6	-1.6 ± 1.6	3.1 ± 1.6
...	...	...	Mean	165.7 ± 1.1	-1.8 ± 1.0	-1.8 ± 1.2	2.5 ± 1.1
SMA	160229	3C273	220.9	10936.5 ± 3.4	368.1 ± 2.8	-556.8 ± 3.8	667.5 ± 3.5
...	...	...	232.9	11202.3 ± 3.9	380.1 ± 4.0	-577.6 ± 4.0	691.5 ± 4.0
...	...	...	Mean	11069.4 ± 2.6	374.1 ± 2.3	-567.2 ± 2.8	679.5 ± 2.6
SMA	Mean	M84	Mean	139.3 ± 22.9	-1.4 ± 0.6	-0.8 ± 0.7	1.6 ± 0.6

REFERENCES

Agudo, I., Thum, C., Gómez, J. L., & Wiesemeyer, H. 2014, A&A, 566, A59

Bietenholz, M. F., Bartel, N., & Rupen, M. P. 2000, ApJ, 532, 895

Blandford, R. D. & Begelman, M. C. 1999, MNRAS, 303, L1

Blandford, R. D. & Konigl, A. 1979, ApJ, 232, 34

Bower, G. C., Backer, D. C., Zhao, J. H., Goss, M., & Falcke, H. 1999, ApJ, 521, 582

Bower, G. C., Dexter, J., Markoff, S., Gurwell, M. A., Rao, R., & McHardy, I. 2015, ApJ, 811, L6

Bower, G. C., Falcke, H., Wright, M. C., & Backer, D. C. 2005, ApJ, 618, L29

Bower, G. C., Wright, M. C. H., Falcke, H., & Backer, D. C. 2003, ApJ, 588, 331

Brentjens, M. A. & de Bruyn, A. G. 2005, A&A, 441, 1217

Brunthaler, A., Bower, G. C., Falcke, H., & Mellon, R. R. 2001, ApJ, 560, L123

Dexter, J. 2016, MNRAS, 462, 115

Dexter, J., McKinney, J. C., & Agol, E. 2012, MNRAS, 421, 1517

Falcke, H. & Biermann, P. L. 1995, A&A, 293, 665

Hull, C. L. H. & Plambeck, R. L. 2015, Journal of Astronomical Instrumentation, 4, 1550005

Hull, C. L. H., Plambeck, R. L., Kwon, W., Bower, G. C., Carpenter, J. M., Crutcher, R. M., Fiege, J. D., Franzmann, E., Hakobian, N. S., Heiles, C., Houde, M., Hughes, A. M., Lamb, J. W., Looney, L. W., Marrone, D. P., Matthews, B. C., Pillai, T., Pound, M. W., Rahman, N., Sandell, G., Stephens, I. W., Tobin, J. J., Vaillancourt, J. E., Volgenau, N. H., & Wright, M. C. H. 2014, ApJS, 213, 13

Johnson, M. D., Fish, V. L., Doeleman, S. S., Marrone, D. P., Plambeck, R. L., Wardle, J. F. C., Akiyama, K., Asada, K., Beaudoin, C., Blackburn, L., Blundell, R., Bower, G. C., Brinkerink, C., Broderick, A. E., Cappallo, R., Chael, A. A., Crew, G. B., Dexter, J., Dexter, M., Freund, R., Friberg, P., Gold, R., Gurwell, M. A., Ho, P. T. P., Honma, M., Inoue, M., Kosowsky, M., Krichbaum, T. P., Lamb, J., Loeb, A., Lu, R.-S., MacMahon, D., McKinney, J. C., Moran, J. M., Narayan, R., Primiani, R. A., Psaltis, D., Rogers, A. E. E., Rosenfeld, K., SooHoo, J., Tilanus, R. P. J., Titus, M.,

Vertatschitsch, L., Weintroub, J., Wright, M., Young, K. H., Zensus, J. A., & Ziurys, L. M. 2015, Science, 350, 1242

Kormendy, J. & Ho, L. C. 2013, ARA&A, 51, 511

Kuo, C. Y., Asada, K., Rao, R., Nakamura, M., Algaba, J. C., Liu, H. B., Inoue, M., Koch, P. M., Ho, P. T. P., Matsushita, S., Pu, H.-Y., Akiyama, K., Nishioka, H., & Pradel, N. 2014, ApJ, 783, L33

Ly, C., Walker, R. C., & Wrobel, J. M. 2004, AJ, 127, 119

Markoff, S., Nowak, M., Young, A., Marshall, H. L., Canizares, C. R., Peck, A., Krips, M., Petitpas, G., Schödel, R., Bower, G. C., Chandra, P., Ray, A., Muno, M., Gallagher, S., Hornstein, S., & Cheung, C. C. 2008, ApJ, 681, 905

Marrone, D. P., Moran, J. M., Zhao, J.-H., & Rao, R. 2006, Journal of Physics Conference Series, 54, 354

—. 2007, ApJ, 654, L57

Marrone, D. P. & Rao, R. 2008, in Proc. SPIE, Vol. 7020, Millimeter and Submillimeter Detectors and Instrumentation for Astronomy IV, 70202B

Mościbrodzka, M., Dexter, J., Davelaar, J., & Falcke, H. 2017, MNRAS, 468, 2214

Mościbrodzka, M., Falcke, H., & Shiokawa, H. 2016, A&A, 586, A38

Mościbrodzka, M., Falcke, H., Shiokawa, H., & Gammie, C. F. 2014, A&A, 570, A7

Narayan, R. & Yi, I. 1995, ApJ, 452, 710

Pang, B., Pen, U.-L., Matzner, C. D., Green, S. R., & Liebendörfer, M. 2011, MNRAS, 415, 1228

Plambeck, R. L., Bower, G. C., Rao, R., Marrone, D. P., Jorstad, S. G., Marscher, A. P., Doeleman, S. S., Fish, V. L., & Johnson, M. D. 2014, ApJ, 797, 66

Rafferty, D. A., McNamara, B. R., Nulsen, P. E. J., & Wise, M. W. 2006, ApJ, 652, 216

Ressler, S. M., Tchekhovskoy, A., Quataert, E., & Gammie, C. F. 2017, MNRAS, 467, 3604

Russell, H. R., McNamara, B. R., Edge, A. C., Hogan, M. T., Main, R. A., & Vantyghem, A. N. 2013, MNRAS, 432, 530

Trippe, S., Neri, R., Krips, M., Castro-Carrizo, A., Bremer, M., Piétu, V., & Fontana, A. L. 2010, A&A, 515, A40

Yuan, F. & Narayan, R. 2014, ARA&A, 52, 529